Acta Oceanol. Sin., 2021, Vol. 40, No. 10, P. 176–186
https://doi.org/10.1007/s13131-021-1841-z
http://www.aosocean.com
E-mail: ocean2@hyxb.org.cn

Inversion of the three-dimensional temperature structure of mesoscale eddies in the Northwest Pacific based on deep learning

Fangjie Yu[1, 2], Zeyuan Wang[1], Shuai Liu[3], Ge Chen[1, 2*]

[1] College of Marine Technology, Faculty of Information Science and Engineering, Ocean University of China, Qingdao 266100, China

[2] Laboratory for Regional Oceanography and Numerical Modeling, Pilot National Laboratory for Marine Science and Technology (Qingdao), Qingdao 266237, China

[3] School of Marine Science and Technology, Tianjin University, Tianjin 300072, China

Received 31 August 2020; accepted 2 April 2021

Abstract

Mesoscale eddies, which are mainly caused by baroclinic effects in the ocean, are common oceanic phenomena in the Northwest Pacific Ocean and play very important roles in ocean circulation, ocean dynamics and material energy transport. The temperature structure of mesoscale eddies will lead to variations in oceanic baroclinity, which can be reflected in the sea level anomaly (SLA). Deep learning can automatically extract different features of data at multiple levels without human intervention, and find the hidden relations of data. Therefore, combining satellite SLA data with deep learning is a good way to invert the temperature structure inside eddies. This paper proposes a deep learning algorithm, eddy convolution neural network (ECN), which can train the relationship between mesoscale eddy temperature anomalies and sea level anomalies (SLAs), relying on the powerful feature extraction and learning abilities of convolutional neural networks. After obtaining the temperature structure model through ECN, according to climatic temperature data, the temperature structure of mesoscale eddies in the Northwest Pacific is retrieved with a spatial resolution of 0.25° at depths of 0–1 000 m. The overall accuracy of the ECN temperature structure is verified using Argo profiles at the locations of cyclonic and anticyclonic eddies during 2015–2016. Taking 10% error as the acceptable threshold of accuracy, 89.64% and 87.25% of the cyclonic and anticyclonic eddy temperature structures obtained by ECN met the threshold, respectively.

Key words: mesoscale eddies, temperature structure, convolutional neural network, Northwest Pacific Ocean

Citation: Yu Fangjie, Wang Zeyuan, Liu Shuai, Chen Ge. 2021. Inversion of the three-dimensional temperature structure of mesoscale eddies in the Northwest Pacific based on deep learning. Acta Oceanologica Sinica, 40(10): 176–186, doi: 10.1007/s13131-021-1841-z

1 Introduction

The temperature structure of seawater is important in research on climate warming, subsurface flow fields and typhoons (Shroyer et al., 2016; Liu and Zhou, 2010; Rao et al., 2010). Temperature shows a nonuniform declining trend with increasing depth (Ge et al., 2017), and the temperature structure of the ocean subsurface cannot be directly observed by satellite . Thus, researching methods for inverting the ocean temperature structure by combining satellite altimetry data with Argo observation data has been an effective way to understand the internal structure of the ocean. An inversion method named the two-layer simplified gravity model (TLM) was proposed by Goni et al. (1996). The TLM has been widely applied in tropical cyclone research and has made important contributions to the study of changes in the upper temperature structure of the ocean. Shay et al. (2000) used the TLM to obtain two isotherms (e.g., the depths of the 20°C and 26°C isotherms) and studied the effects of warm oceanic features on Hurricane Opal. The Modular Ocean Data Assimilation System (MODAS) is used by the U.S. Navy to obtain three-dimensional fields of temperature and salinity in the global ocean. The MODAS could predict the subsurface structure by constructing synthetic profiles, which is formed through regression method using *in situ* observations data, such as sea surface height (SSH) and sea surface temperature (SST). The resolution of MODAS is (1/2)° in the open ocean, (1/4)° in coastal regions, and (1/8)° near land (Fox et al., 2002). The ARMOR3D product launched by CMEMS, which combines satellite remote sensing data (SLA and SST) with *in situ* observations using regression and optimal interpolation, could provide weekly 3D combined temperature and salinity fields on a (1/4)° horizontal regular grid with 33 unevenly spaced layers between the surface and 5 500 m depth (Guinehut et al., 2012; Barcelo-Llull et al., 2018). With the development of satellite sensors, more detailed sea surface data can be obtained, which greatly improves the understanding of the surface ocean. At the same time, more detailed information on the subsurface ocean is urgently required. To better study the marine upper layer characteristics, Pun et al. (2014, 2016) proposed a new derivation method that increases the vertical resolu-

Foundation item: The National Key Research and Development Program of China under contract Nos 2016YFC1402608, 2016YFC1400904, 2016YFC1400900 and 2019YFD0901000.
*Corresponding author, E-mail: gechen@ouc.edu.cn

tion of the temperature structure to 26 isotherms and used this method to study tropical cyclones in the Pacific Ocean and the Atlantic Ocean. As deep learning has performed well in the analysis and mining of time-series data (Hinton and Salakhutdinov, 2006; Mandal et al., 2005; Corchado and Aiken, 2002), it has been applied to study the ocean temperature structure, and relatively accurate results were obtained (Yang et al., 2018; Zhao and Han, 2015). Ali et al. (2004, 2012) predicted the temperature structure of the Arabian Sea at depths of 0–300 m through a neural network, and 50% of the estimations were within an error of 0.5°C, while 90% were within 1.0°C. In 2012, he used temperature profiles obtained by neural network to calculate tropical cyclone heat potential, which could help to improve tropical cyclone heat potential. Su et al. (2018, 2019) used the Random Forest method and XGBoost model to predict the thermohaline structure of the global ocean at depths of 0–2 000 m, which greatly extended the prediction depth, and the average NRMSE value of the estimated temperature anomaly was 0.035. Han et al. (2019) proposed a convolutional neural network method to estimate subsurface temperature. The average MSE of estimation is 0.406 6 and the average R^2 is 0.964. Zhang et al. (2020) proposed a multilayer convolutional LSTM method, which could predict the temperature from 0 m to 2 000 m, and the RMSE of the prediction was approximately 0.2. The above results show that the large-scale ocean thermohaline structure can be predicted well by using machine learning algorithms. However, for regions that exhibit complex mesoscale phenomena, the accuracy of the temperature structure would be affected (Pun et al., 2007). To solve this problem, Pun et al. (2014) divided their study area according to the frequency of mesoscale eddies and established regression models. Similarly, Lu et al. (2019) used clustering to partition study areas covering the global ocean before predicting the temperature structure and found that the subsurface temperature predicted by this preclustering method could reflect mesoscale phenomena better than that without preclustering.

Nevertheless, dividing a region according to the frequency of mesoscale phenomena therein and studying those regions separately could improve the accuracy of the temperature structure. Mesoscale dynamics, such as mesoscale eddies, are common phenomena throughout the global ocean and have complex three-dimensional structures, various shapes and strong nonlinear factors (Shang et al., 2013). Thus, instead of distinguishing the eddy zone, it would be more precise to build a special temperature structure model for mesoscale eddies. In this context, a convolutional neural network (CNN), one of the most successful models in deep learning applications (LeCun et al., 2015), has been used in the prediction of sea surface data (e.g., SST and SSHA) and the identification of ocean fronts (Ducournau and Fablet, 2016; Lima et al., 2017; Barth et al., 2020; Song et al., 2020), and it was found that the efficiency and accuracy could be improved compared to traditional forecasting methods (Alvera-Azcárate et al., 2005; Yang et al., 2016). Therefore, due to the nonlinear nature of mesoscale eddies, introducing deep learning to improve the mesoscale three-dimensional eddy temperature structure is feasible (Su et al., 2018).

In this paper, a deep learning method is proposed to invert mesoscale three-dimensional eddy temperature structures using satellite altimetry data and Argo profile data. The second section describes the data set, and the deep learning inversion method is introduced in the third section. The inversion method is verified in the fourth section. Finally, the conclusion and some future prospects are presented in the fifth section.

2 Data

2.1 *Argo*

The Argo network of observation is widely distributed throughout the global ocean (Long et al., 2015). These floats can continuously monitor the ocean temperature, salinity and depth within 10 days to obtain high-resolution data. The global ocean currently contains more than 3 800 free-floating buoys. Thus, Argo observations can provide real-time and high-quality *in situ* data on a global scale.

The Argo data used was from French Research Institute for the Exploitation of the Seas (IFREMER) and the dataset is a global dataset. This study selected 0°–60°N, 105°–180°E as the study area, and downloaded 13 years of data from 2003 to 2016. Among them, the profiles from 2003 to 2014 were used to establish the neural network training model, while the profiles from 2015 and 2016 were used to verify the accuracy of the inversion method. The unit of temperature is °C.

Before using the data, it is necessary to control the quality of the Argo data to make the research results more reliable. Specifically, the Argo data contain the following: the range of temperature data points first observed in the Argo profile; the maximum and minimum depths observed by Argo; the minimum number of effectively observed data points in the observation data; and the minimum temperature difference between adjacent interval points and the maximum depth difference between adjacent interval points in the upper observation section. Statistically, approximately 12% of all Argo profile data were excluded. The specific quality control process of Argo profile is shown in Table 1.

Table 1. Argo profile quality control process

Quality control items	Thresholds
Temperature at the first observation point	>0°C and <35°C
Maximum observed depth	>200 m
Number of valid points	>10
Temperature difference between adjacent interval points	<1°C
Maximum depth interval between adjacent points	<300 m

2.2 *Satellite data*

This paper also employed satellite altimetry data, including mean absolute dynamic topography (MADT) and sea level anomaly (SLA) data. The MADT is the sum of the SLA and mean dynamic topography (MDT). These altimetry data were obtained from AVISO provided by the French National Space Research Center, and the data set is integrated with altimetry data from Topex/Poseidon, Jason-1 and Jason-2, GFO, Envisat, ERS-1/2 and other satellites. The temporal resolution of the data is 1 day, and the spatial resolution is 0.25°×0.25°. MADT data were used to identify mesoscale eddies, while SLA data were used to invert the temperature structure of mesoscale eddies.

In order to avoid affecting the observation accuracy due to the absorption of floating objects on the sea surface, the CTD sensor carried by Argo will stop working when it rises to about 5 m to the sea surface during the observation of the oceanographic thermohaline profile. Therefore, the shallowest depth that Argo can observe is about 5 m to 10 m from the sea surface. Therefore, to complete the temperature structure for this research, 14 years (2003–2016) of daily SST data were downloaded from RSS (http://

www.remss.com/) as a substitute for the surface ocean temperature.

2.3 *WOA climate state data*

WOA13, published in 2013, is an integrated data set for the long-term objective analysis of the global ocean. This data set contains many important climatic factors, such as temperature, salt, phosphate, dissolved oxygen, nitric acid and silicate, and is widely used in ocean general circulation models (OGCMS). WOA13 makes some modifications and improvements to previous versions, from which data is also integrated. The data set has different temporal resolutions at scales of 1 year, 3 months, and 1 month and has spatial resolutions of 5°, 1° and 0.25°.

WOA climate state data were used as a baseline to describe temperature changes in the ocean. The temperature anomaly is the temperature measured by Argo minus the WOA climatic temperature, which represents the change in the point relative to the inter-annual average temperature. The calculation formula is shown below. And then the temperature anomaly was used for model training.

$$T_{\text{anomaly}(x,y,z)} = T_{\text{Argo}(x,y,z)} - T_{\text{WOA}(x,y,z)}, \quad (1)$$

where x and y is the longitude and latitude of mesoscale eddy, z is the depth.

2.4 *Mesoscale eddy identification and Argo data selection*

Based on this eddy identification algorithm, a mesoscale eddy data set is constructed for the western Pacific from 2003 to 2016, and the eddies with Argo data were filtered out according to the position of Argo. The detailed information is shown in Fig. 1.

3 Methods

This paper proposes a new algorithm based on a neural network architecture named the eddy convolution neural network (ECN), which contains a sample input layer, training convolutional layer, feature pooling layer, locally normalized layer, feature connection layer, and final output layer. Figure 2 shows the structure for the ECN, which is composed of 5 convolutional layers and 1 full connection layer. The dimension of the first convolutional layer is set to 5×5×5, the second to fourth layers are 10×5×5, and the last layer is 20×5×5. The dimension of convolution kernels in each layer is 2×2, and the step size is 1. Since the size of the output feature maps is 5×5, which is same as input, the edge filling method is used to fill the missing area of the matrix. In this paper, 0 is used to fill the edge. Meanwhile, the number of convolution kernels is consistent with the number of output feature graphs, so there are 5 convolution kernels in the first convolution layer, 10 convolution kernels in the second to the fourth layer, and 20 convolution kernels in the fifth layer. After 5 layers of convolution operation, the matrix data is converted into one-dimensional data and input to the fully connected layer, and finally the output data is obtained. To obtain the optimized model, the ECN model uses Xavier weight initialization method to prevent vanishing gradient or exploding gradient by making the variances of each layer as equal as possible. In order to prevent the occurrence of overfitting, L2 regularization, Dropout and Early Stopping are used in the ECN model. As for the activation function, Tanh (hyperbolic tangent function) function can solve the zero-mean problem, but it consumes a lot of computing resources. Relu (Rectified Linear Unit) function can effectively solve gradient saturation and dispersion problems, but when the learning rate is too high and parameter update is too large, some neurons may fail to activate. Therefore, Tanh function is used in the first two convolutional layers of the ECN model, while Relu function is selected as the activation function in the third to the fifth convolutional layer and the last fully connected layer. Some selected hyperparameters are shown in Table 2.

First, the MADT data from 2003 to 2016 were used to identify mesoscale eddies, and mesoscale eddies with Argo data were extracted. Then, SLA training dataset and test data set were made according to the mesoscale eddies with Argo data, so that the mesoscale eddies, Argo data and SLA data are matched in time and space. The SLA training data were divided according to the eddy polarity into 8 502 cyclonic eddies and 8 762 anticyclonic eddies from 2003 to 2014. In the training data set, the SLA data at each eddy were arranged into a 5×5 matrix composed of the SLA values at and around the eddy center.

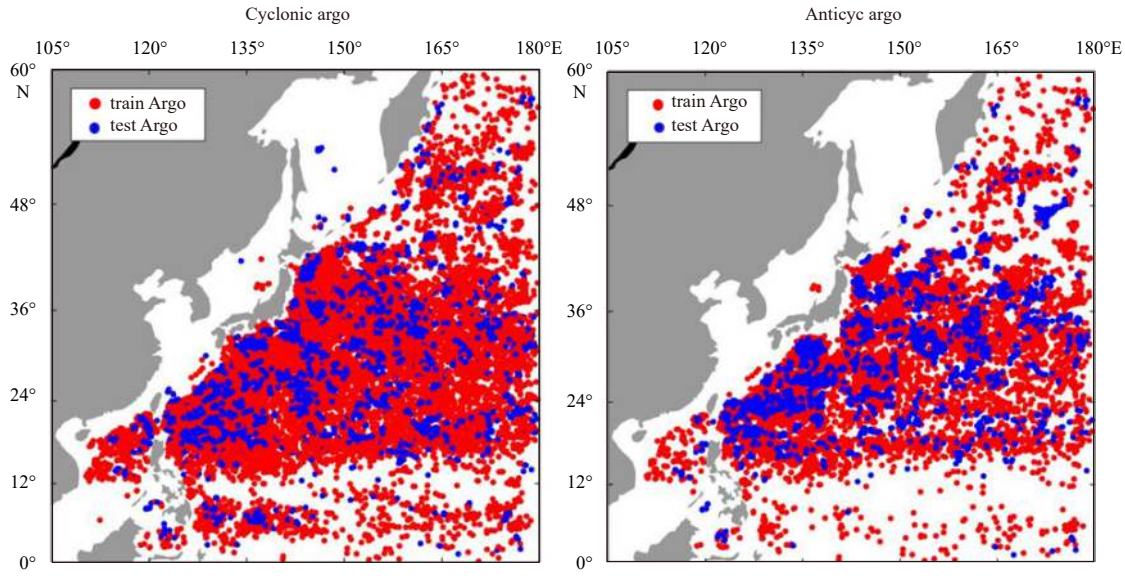

Fig. 1. The distribution of selected Argo data. The red points are the training data from 2003 to 2014, and the blue points are the test data from 2015 to 2016.

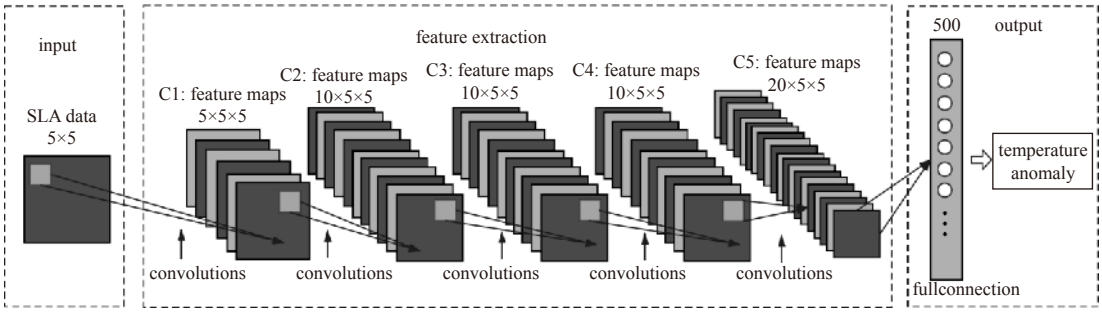

Fig. 2. The structure of ECN for obtaining temperature anomaly.

Table 2. Some selected hyperparameters

Parameter	Optimal value
Activation_function	Tanh, Relu
Weights initialization	Xavier
Learning rate	0.001
Decay	Adam
Batch size	128
Loss function	MSE
Dropout	0.8
Regularization	L2
Early stopping	True

Second, the training data were used to train the ECN model, and a suitable temperature anomaly model was obtained. With the SLA and temperature anomaly data as the original input and target output, the ECN is divided into a depth range of 5–1 000 m into 46 layers, and the model is trained layer by layer.

Third, the SLA test data (2 564 cyclonic test samples and 3 414 anticyclonic test samples from 2015 to 2016) and WOA data were input into the model to obtain the temperature structure inversion results. Then, substituting SST as the temperature value at 0 m into the temperature structure, a temperature structure of 47 layers in total from 0–1 000 m can be obtained.

4 Evaluation of the results

This paper selected SLA and temperature anomaly data from 2003 to 2014 for training and obtained ECN models for 46 layers respectively. SLA and temperature anomaly data from 2015 to 2016 did not participate in the model training process; rather, these data were used as a test set to quantitatively evaluate various characteristics of the inversion model. Moreover, the inversion results of the temperature profile obtained by the ECN were compared with those obtained by an existing linear regression (Linear-reg) method (Pun et al., 2014) and back propagation neural network (BPNN) model (Zhao and Han, 2015).

4.1 *Comparison between observed values and inversion results*

4.1.1 *Comparison of cyclonic eddies*

The SLA data of the cyclonic eddies from 2015 to 2016 were imported into the ECN model to obtain the temperature anomaly ($\Delta T'_{i,k}$) at each eddy layer. The results of the cyclonic eddy temperature anomaly ($\Delta T'$) obtained by the ECN model are compared with the temperature anomaly (ΔT) observations obtained by Argo, as shown in Fig. 3. Figure 3a shows the results of a comparison between the values of $\Delta T'$ and ΔT at 30 m for 2 564 cyclonic eddies. The red points represent the ECN-predicted values at a depth of 30 m, while the green points represent the true values observed by Argo. From the figure, it is obvious that the SLA values at cyclonic eddies are mostly negative. The distribution of temperature anomalies of cyclonic eddies in the vertical direction is basically negative, and with increasing depth, the temperature anomalies gradually weaken and tend to zero. Furthermore, the accuracy of the model will decrease when the absolute SLA value is small and the temperature anomaly is large. Normally, the SLA in the eddy area is not equal to zero. The larger the SLA amplitude is, the stronger the mesoscale eddy is. There are two possibilities for the SLA in the eddy area approaching zero. One is that there is another upper ocean dynamic process which causes the sea level change opposite to those caused by the mesoscale eddy. The second is that the eddy signal is weak, resulting in very little change in sea level. Therefore, there will be some errors in these two cases. For most SLA input signals, the ECN model has a good inversion ability for the cyclonic eddy temperature structure. The inversion results of the ECN model at 100 m, 175 m, 300 m, 450 m and 750 m are shown in Figs 3b–f, respectively. These findings indicate that the deep learning ECN model trained in this paper has learned certain characteristics of the SLA data and the temperature anomaly structure of the cyclonic eddies in this region with a good inversion ability for latter.

Figure 4 shows the comparison of the temperature profiles at depths of 5–1 000 m in the cyclonic eddies obtained by the ECN model, BPNN model, linear regression model and *in situ* Argo. Profiles in different months from 2015 to 2016 are randomly selected according to the season. From Fig. 4, compared with the profiles obtained by linear regression method, the profile obtained by deep learning method is closer and more accurate to Argo profile. Meanwhile, the detailed changes of temperature structure can be reflected more accurately, which proves that deep learning method has obvious advantages in nonlinear inversion. In addition, it can be clearly seen that the accuracy of the results obtained by BPNN method fluctuates greatly in some depths, while the ECN model proposed in this paper can make the inversion results at each depth layer more stable and accurate. The gradient descent method used by BPNN can make the network weight converge to the local minimum, but it cannot guarantee that the local minimum is the global minimum, which will lead to a large error in the inversion results of some depth layers. To solve this problem, the ECN model uses Adam method to determine the learning rate. Different from the traditional gradient descent algorithm, which has a single and constant learning rate, Adam (Adaptive moment estimation) method can adaptively calculate the learning rate of each parameter in the process of iterative training so as to avoid the occurrence of the local optimal situation.

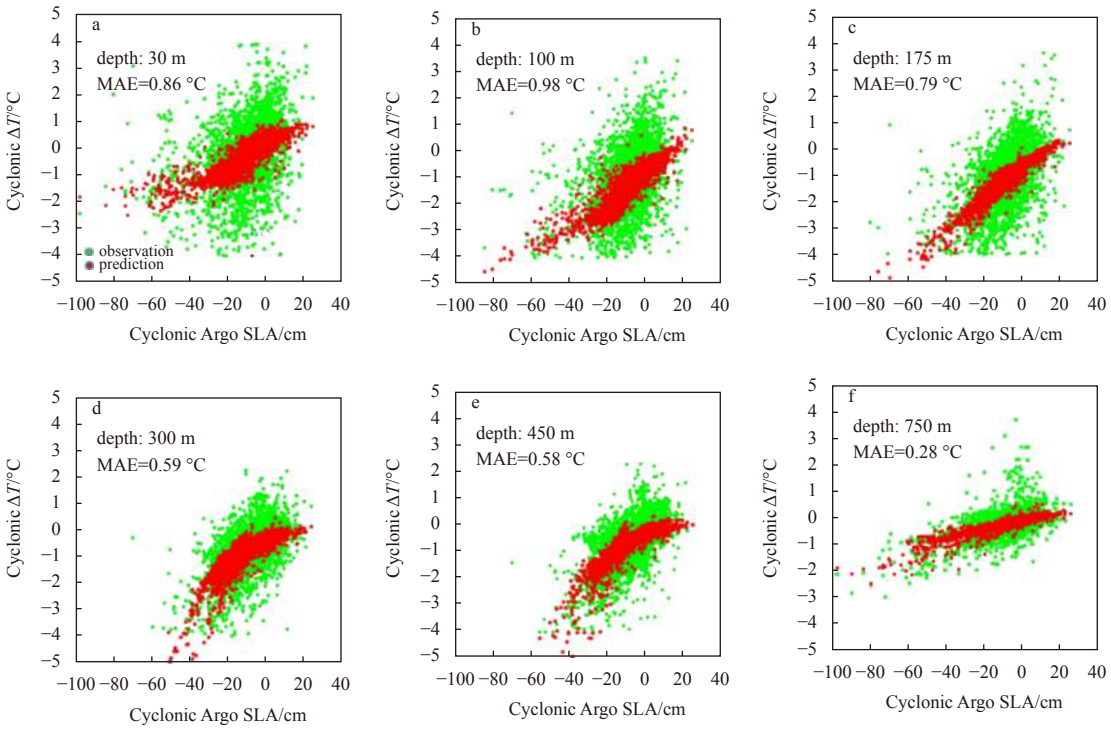

Fig. 3. Comparison between the inversion cyclonic eddy temperature anomalies (red) at depths of 30 m (a), 100 m (b), 175 m (c), 300 m (d), 450 m (e) and 750 m (f) obtained by the ECN model and temperature anomalies (green) observed by Argo of 2 564 cyclonic eddies at the same position.

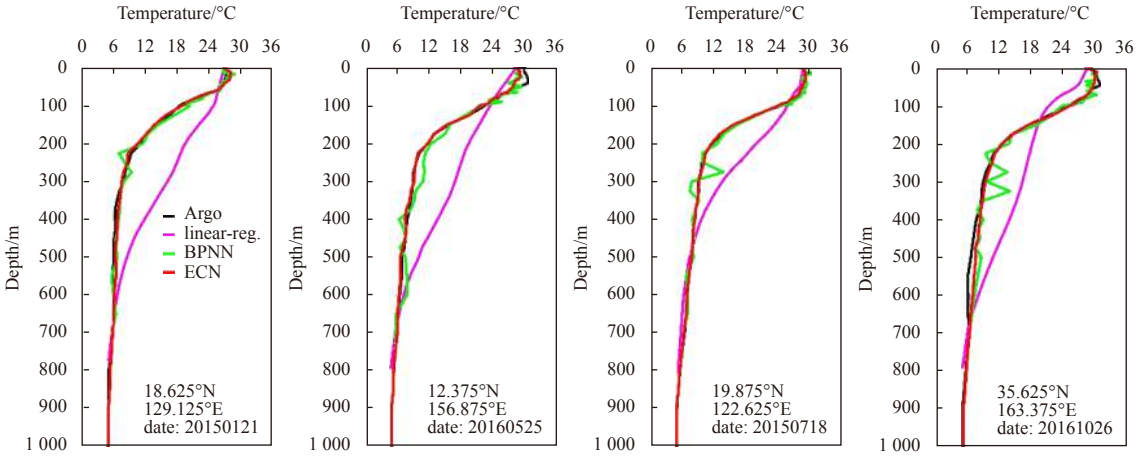

Fig. 4. Comparison among the temperature profiles at depths of 0–1 000 m at the cyclonic eddies obtained by linear regression model (magenta), BPNN (green), ECN (red) and Argo (black). Profiles are selected randomly according to the season.

4.1.2 *Comparison of anticyclonic eddies*

In the same way, the SLA data at the anticyclonic eddies from 2015 to 2016 were imported into the ECN model, and the temperature anomalies ($\Delta T'_{i,k}$) of the eddies in each layer were obtained. The results of the anticyclonic eddy temperature anomaly ($\Delta T'$) obtained by the ECN model are compared with the temperature anomaly (ΔT) obtained by Argo in Fig. 5. In Fig. 5a, the red points represent the ECN-predicted values at a depth of 30 m, while the green points represent the true values observed by Argo. As opposed to those of the cyclonic eddies, the SLA values of the anticyclonic eddies are mostly positive. Furthermore, the distribution of temperature anomalies of the anticyclonic eddies in the vertical direction is basically positive, and with increasing depth, the temperature anomalies gradually weaken and tend to zero. Similarly, when the absolute SLA value is small and the temperature anomaly is large, the accuracy of the model will decrease in rare cases. However, for most SLA input signals, the ECN model has a good inversion ability for the anticyclonic eddy temperature structure. The inversion results of the ECN model at 100 m, 175 m, 300 m, 450 m and 750 m are shown in Figs 5b–f, respectively, similarly showing that the ECN model has a good inversion ability for the anticyclonic temperature structure.

Similarly, Figure 6 shows a comparison among the temperature profiles at depths of 5–1 000 m of the anticyclonic eddies obtained by the ECN model, the BPNN model, the linear regression model and Argo. From this figure, compared with the profiles obtained by linear regression model and BPNN model, it is obvious

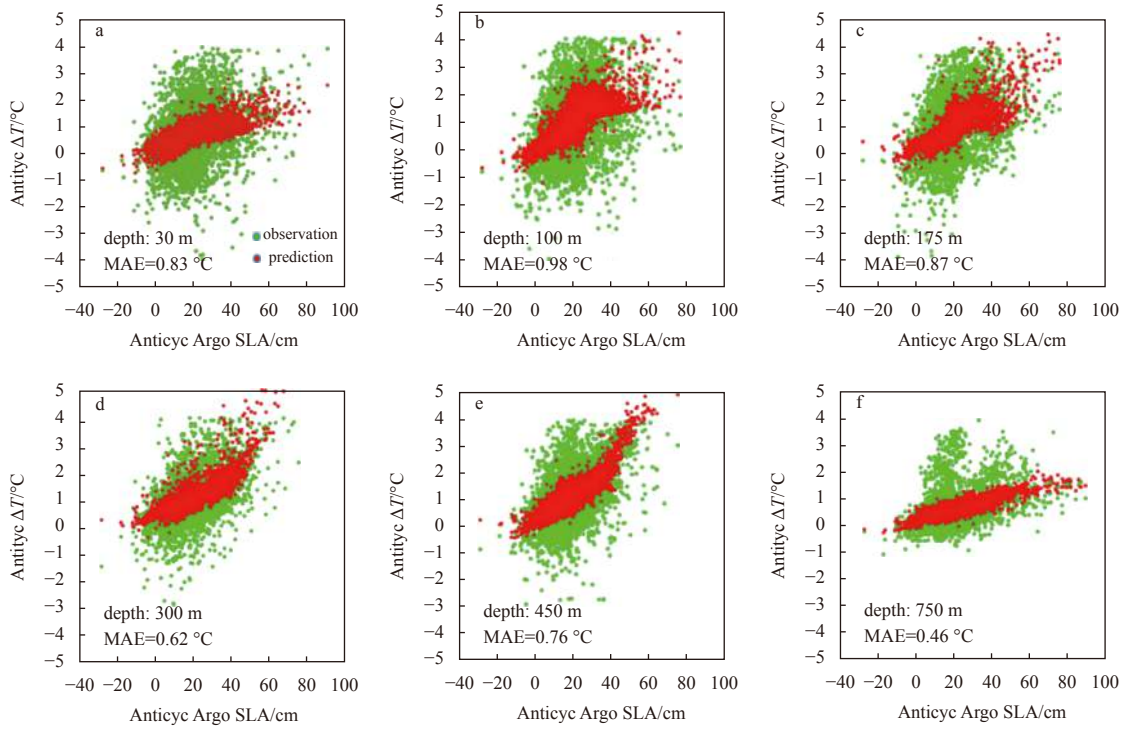

Fig. 5. Comparison between the inversion anticyclonic eddy temperature anomalies (red) at depths of 30 m (a), 100 m (b), 175 m (c), 300 m (d), 450 m (e) and 750 m (f) obtained by the ECN model and temperature anomalies (green) observed by Argo of 2 564 anticyclonic eddies at the same position.

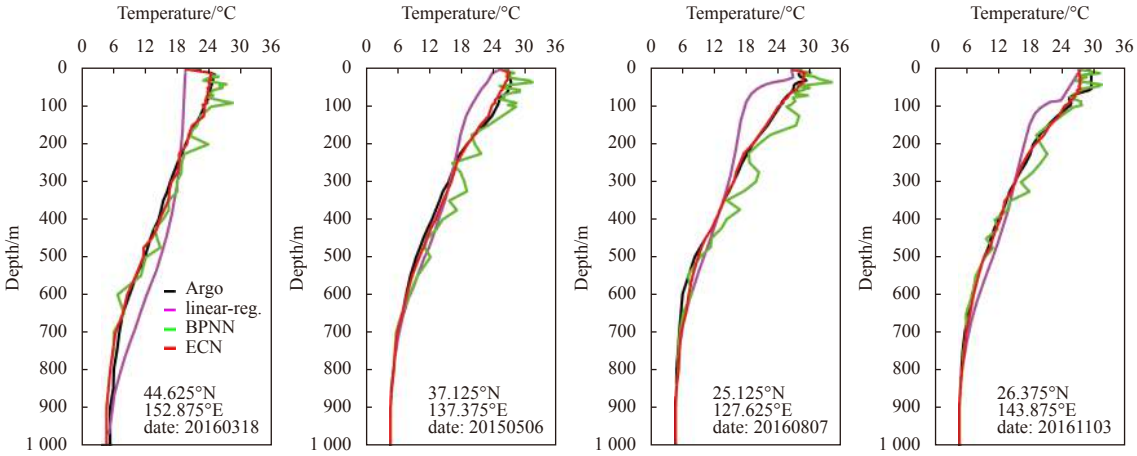

Fig. 6. Comparison among the temperature profiles at depths of 0–1 000 m at the anticyclonic eddies obtained by linear regression model (magenta), BPNN (green), ECN (red) and Argo (black). Profiles are selected randomly according to the season.

that the inverted anticyclonic eddy profile obtained by the ECN model is very close to the measured profile and is consistent with the measured profile, confirming that the inversion results of the ECN model for anticyclonic eddies are also highly accurate. In addition, the gaps in the surface ocean temperature are filled with SST data, so it is inevitable that there will be some errors, which will lead to the deviation of the inversion results at the sea surface. However, the proposed method retains the integrity of the profile.

4.2 *Analysis of evaluation indexes of results*

To quantitatively analyze the performance of the ECN model, several evaluation indicators were selected to analyze the accuracy of the ECN model.

(1) RMSE (root mean square error), namely, the root mean square error between the predicted value ($\Delta T^{'}$) and observed value (ΔT), evaluates the accuracy of the ECN model.

$$\mathrm{RMSE} = \sqrt{\frac{1}{N}\sum_{i=1}^{N}\left(\Delta T_i^{'} - \Delta T_i\right)^2}. \tag{2}$$

(2) MAE (mean absolute error), namely, the mean of the absolute error, reflects the dispersion degree between $\Delta T^{'}$ and ΔT.

$$\mathrm{MAE} = \frac{1}{N}\sum_{i=1}^{N}\left|\Delta T_i^{'} - \Delta T_i\right|. \tag{3}$$

(3) R (correlation coefficient) reflects the correlation between $\Delta T^{'}$ and ΔT.

$$R=\frac{\sum_{i=1}^{N}(\Delta T_i^{'}-\Delta\overline{T^{'}})(\Delta T_i-\Delta\overline{T})}{\sqrt{\sum_{i=1}^{N}(\Delta T_i^{'}-\Delta\overline{T^{'}})^2}\sqrt{\sum_{i=1}^{N}(\Delta T_i-\Delta\overline{T})^2}}. \quad (4)$$

(4) Error. The proportion of the RMSE in the actual mean observed temperature (MOT) of Argo was defined as error to reflect the accuracy of the model.

$$\text{Error}=\frac{\sqrt{\frac{1}{N}\sum_{i=1}^{N}(\Delta T_i^{'}-\Delta T_i)^2}}{\overline{T}}\times 100\%=\frac{\text{RMSE}}{\text{MOT}}\times 100\%. \quad (5)$$

$$\text{MOT}=\frac{1}{N}\sum_{i=1}^{N}T_i. \quad (6)$$

4.2.1 *Evaluation index analysis of cyclonic eddy*

First, cyclonic eddy accuracy charts of the temperature data predicted by the ECN model and the temperature data obtained by Argo were drawn (Fig. 7). The unit of temperature is °C. The depth range includes 30 m (a), 100 m (b), 175 m (c), 300 m (d), 450 m (e), and 750 m (f). Figure 7 shows some of the calculation results for the evaluation indexes. The x-coordinate is the temperature of the cyclonic eddy measured by Argo, and the y-coordinate is the predicted temperature obtained by the ECN model. The y=x line is also drawn to demonstrate that the accuracy of the ECN model is high if the points are close to the line. If the color is close to red, the dots are denser. For example, the RMSE is 1.14 and the MAE is 0.86 from Fig. 7a. Figure 7 shows that the accuracy of the ECN model is affected by the depth. The results of the ECN model are within a reasonable range of Error.

The accuracy chart above shows a partial depth analysis for cyclonic eddies. The ECN model can invert the temperature structure of cyclonic eddies with a total of 46 layers in the depth range of 5–1 000 m; the accuracy was also analyzed in all depth layers. Figure 8 shows the accuracy of the cyclonic eddy temperature in all depth layers. From Fig. 8a, the RMSEs of most depths are within 1°C. The RMSEs are small at depth, and even in the superficial layers, the RMSEs are within 1.3°C, that is, within an acceptable range. According to Fig. 8a, there is a "bump" within the depth of 50–200 m. The reason for this phenomenon may be related to the depth of mixing layer. In the Northwest Pacific Ocean, the depth of the mixing layer is about 50–100 m (de Boyer Montégut et al., 2004), and there is no significant change in temperature at this depth, so the RMSE of this depth is small. However, the temperature of the sea water in the thermocline will have a large change, so the RMSE will be large when the temperature structure of the thermocline is inversion, which is the reason for the "bump" in Fig. 8a. Figure 8b shows the variation in the MAE, which has a similar pattern to the RMSE and reflects the low dispersion between the predicted and actual temperatures. Figure 8c shows the correlation between the ECN-predicted temperature anomaly and the temperature anomaly observed by Argo in each depth layer; the correlation reflects the quality of the ECN model. The overall correlation coefficient is relatively high, whereas the correlation is low only in the mixed layer and the deep ocean. Figure 8d shows the percentage of the RMSE in the mean actual observed temperature ($\overline{T}$); the error tends to increase first and then decrease, but most of the errors are within 10%. According to the analysis of these evaluation indexes, the ECN model can establish a complete and accurate temperature anomaly structure for cyclonic eddies and then combine that structure with climate state data of the temperature and SST to obtain a complete temperature profile for cyclonic eddies.

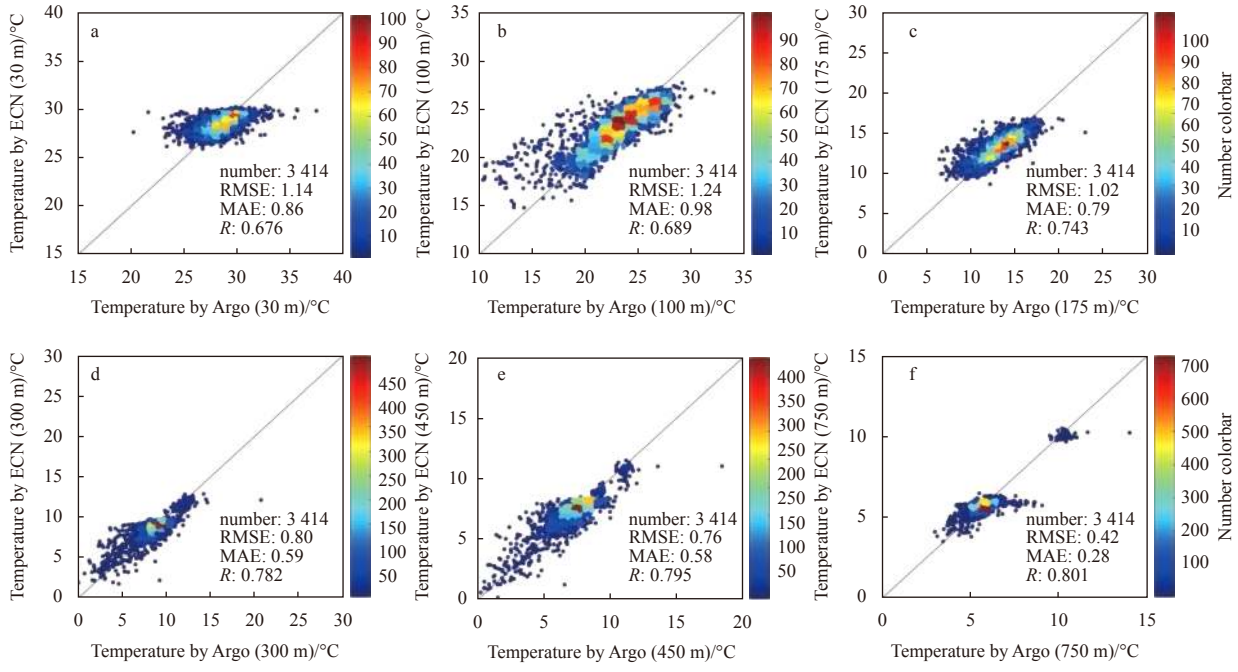

Fig. 7. Accuracy analysis of the ECN model for cyclonic eddies. Depths of 30 m (a), 100 m (b), 175 m (c), 300 m (d), 450 m (e) and 750 m (f).

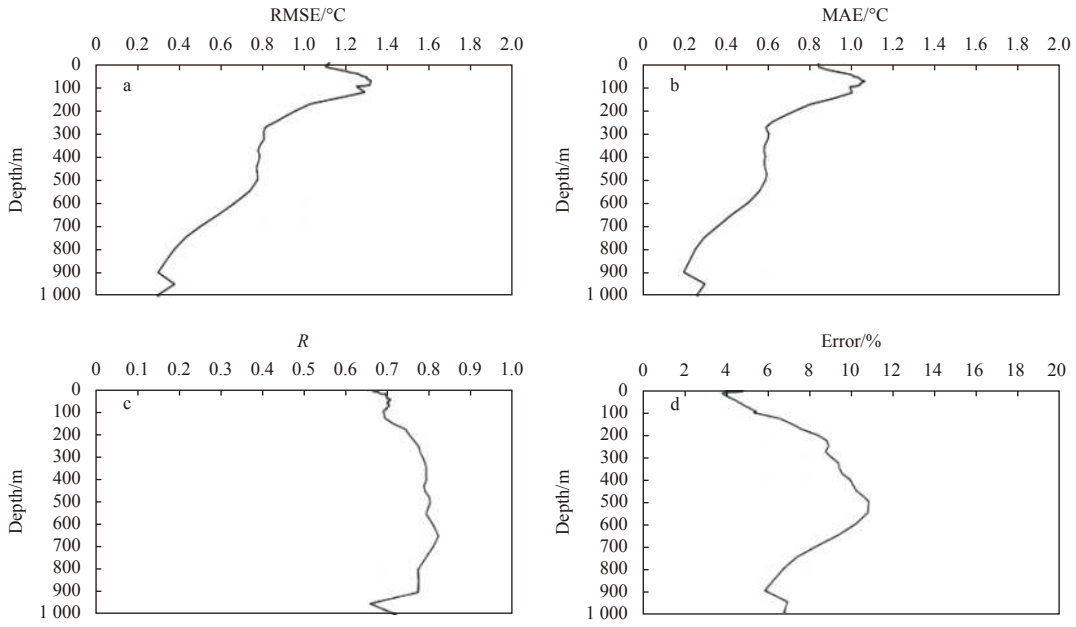

Fig. 8. RMSE (a), MAE (b), *R* (c), and Error (d) for cyclonic eddies.

4.2.2 *Evaluation index analysis of anticyclonic eddy*

Similarly, accuracy charts were drawn between the temperature of anticyclonic eddies obtained by the ECN model and the measured temperature observed by Argo (Fig. 9). The depth range includes 30 m (a), 100 m (b), 175 m (c), 300 m (d), 450 m (e), and 750 m (f). Similar to cyclonic eddies, the accuracy of the model is affected by depth and has a certain regularity. Additionally, the ECN model results for anticyclonic eddies are in a reasonable error range.

The ECN model was used to invert the temperature structure of anticyclonic eddies with 46 layers at depths from 5 m to 1 000 m. Figure 10 shows the accuracy of the anticyclonic eddy temperature in all depth layers. The RMSE and MAE of anticyclonic eddies are similar to those of cyclonic eddies and are also in acceptable ranges. According to the R values, the overall correlation coefficient is high, while it is somewhat low only in the mixed layer. The Error also tends to increase first and then decrease, and most of them are within 10%. Similarly, according to the analysis of these evaluation indexes, the ECN model can produce a complete and accurate temperature anomaly structure for anticyclonic eddies; then, combined with climate state data of the temperature and SST, a complete temperature profile structure of

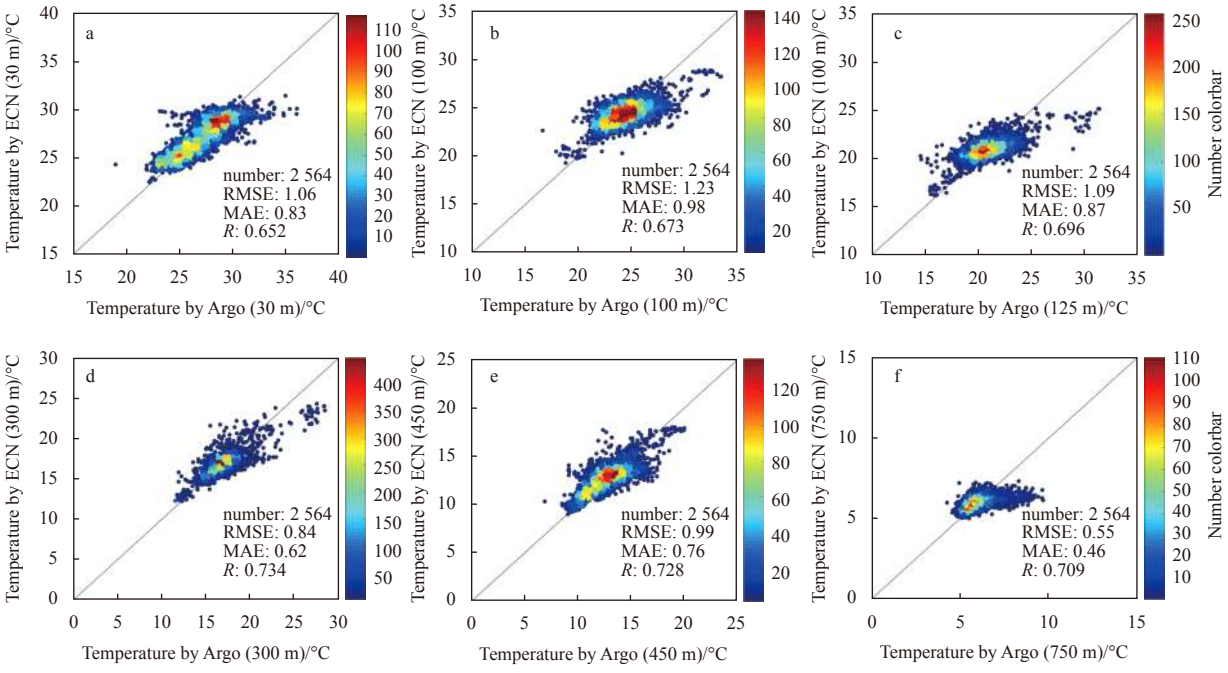

Fig. 9. Accuracy analysis of the ECN model for anticyclonic eddies. Depths of 30 m (a), 100 m (b), 175 m (c), 300 m (d), 450 m (e) and 750 m (f).

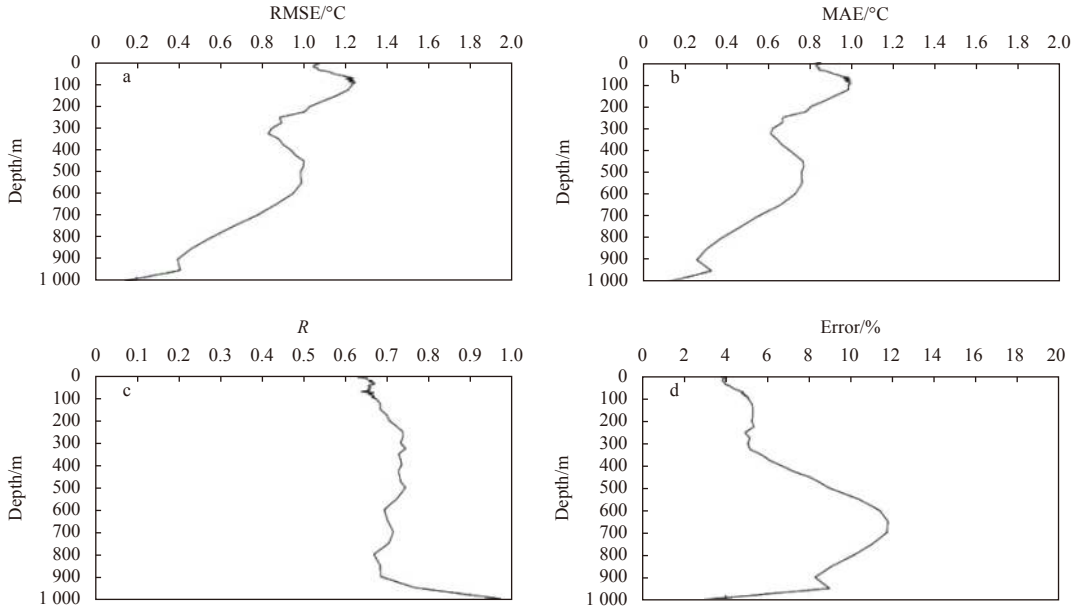

Fig. 10. RMSE (a), MAE (b), *R* (c), and Error (d) for anticyclonic eddies.

anticyclonic eddies can be obtained. In conclusion, according to the evaluation indexes of the inversion results, the ECN model has the ability to invert mesoscale eddies in the Northwest Pacific.

4.3 *Monthly accuracy analysis of results*

In the previous section, the discrete, accurate and relevant results of the ECN model for cyclonic eddies and anticyclonic eddies are quantitatively described and analyzed. The previous content proves that the ECN model is applicable overall to cyclonic eddies and anticyclonic eddies. This section mainly aims at the inversion results of data in different months to verify the monthly applicability of the ECN model.

4.3.1 *Monthly accuracy analysis of cyclonic eddies*

The cyclonic eddy accuracy of the ECN model in every month and the ensemble average for the Northwest Pacific Ocean are verified by quantitative analysis (Fig. 11). As shown in Fig. 11, for each month, the accuracy of the ECN model for cyclonic eddies is different. Figure 11a shows the RMSE between the inversion results and the observed values of cyclonic eddies from January to December and the ensemble average value. As seen from the figure, the RMSE of cyclonic eddies is relatively similar in each month from January to December, especially in the deep ocean, and has the same regularity. However, in the ocean above 600 m, the RMSE in each month is different. It can be clearly seen that for cyclonic eddies, the RMSE is larger in April, May and September but smaller in June and July. Figure 11b shows the Error for cyclonic eddies during January and December. The errors in each month are relatively close at all depths, but the errors in April and May are larger than those in the other months, and the errors in June and July are the smallest, indicating that the accuracy of the ECN model varies from month to month.

To quantify the difference in accuracy of the ECN model at different depths in different months, this paper decided to take Error as the threshold for judgment. The evaluation threshold is selected as 10% error to determine the accuracy at different depths in each month. In the shallow ocean, the error range of the ECN model can be applied to all months, while in the deeper ocean, the Error is slightly higher than the threshold. The reason for this problem may be that the percentage of the RMSE in the observed temperature mean increases as the observed temperature mean decreases with increasing depth. In general, 89.64% of the cyclonic eddies obtained by the ECN model met the accuracy threshold.

4.3.2 *Monthly accuracy analysis of anticyclonic eddies*

A quantitative analysis was conducted on the accuracy of the anticyclonic eddy temperature inversion results obtained by the ECN model in each month for the Northwest Pacific Ocean (Fig. 12).

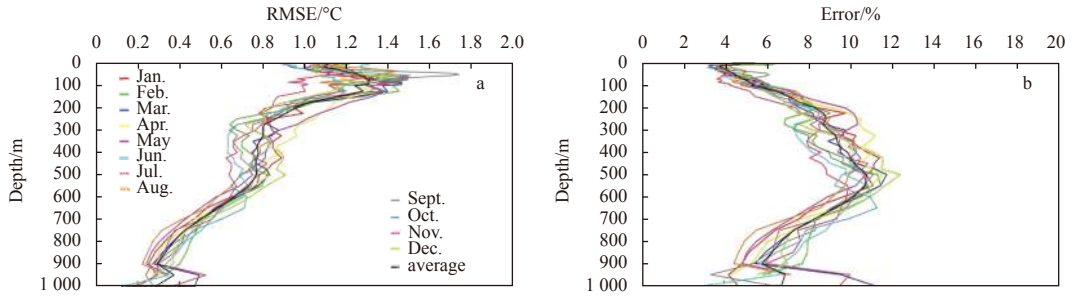

Fig. 11. The RMSE and Error of each month for cyclonic eddies.

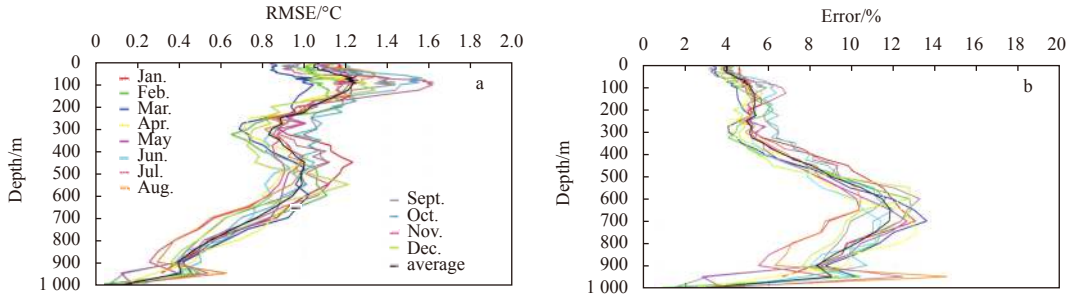

Fig. 12. The RMSE and Error of each month for anticyclonic eddies.

The accuracy of the temperature inversion results obtained by the ECN model also differs in each month. Figure 12a shows the RMSE between the temperature anomaly inversion results and observed values for anticyclonic eddies from January to December and the ensemble mean value. As seen from this figure, in the period from January to December, the RMSE of the anticyclonic eddies basically has the same trend in each month, and in the deep ocean, the RMSE has the same regularity but varies monthly. For anticyclonic eddies, the RMSE is larger in October and November and smaller in February and March. Figure 12b shows the percentage of the RMSE in the observed actual temperature, namely, the Error, for anticyclonic eddies from January to December. In the upper ocean, the Error in each month is relatively similar, but the Errors in July and November are generally larger than those in other months, while the Errors in February and August are generally smaller, indicating that the inversion accuracy of the ECN model in each month for anticyclonic eddies differs.

Similarly, Error was again chosen as the threshold for quantifying the ECN model inversion accuracy in different depth layers in different months, and 10% Error was again taken as the threshold. For anticyclonic eddies, the error range of the ECN model can also be applied to all months in the shallow ocean, while some months cannot meet this requirement for the deeper ocean. In general, 87.25% of the anticyclonic eddy results obtained by the ECN model reached the accuracy threshold.

5 Summary

The deep learning algorithm proposed in this paper, ECN, was utilized to invert the mesoscale three-dimensional eddy temperature structure in the Northwest Pacific Ocean, and the inversion results of the model were quantitatively analyzed according to evaluation indexes. The main significance of this study is as follows:

(1) The western Pacific Ocean has unique regional marine features and is one of the areas with the highest concentration of mesoscale eddies (Wu et al., 2016). However, there is a lack of *in situ* measurement data in the tropical cyclone (TC) orbit area to describe the three-dimensional structure of mesoscale eddies. The deep learning was introduced to deduce and invert the mesoscale eddy temperature structure, thereby obtaining 47 layers over depths from 0 m to 1 000 m. The structure has a daily resolution and a horizontal resolution of 0.25°. Compared with existing inversion methods, the results of this paper are described in more detail with better spatial and temporal resolutions.

(2) An independent Argo profile data set was used for verification, and it was found that the ECN model achieves good accuracy for the temperature inversion of mesoscale eddies in the Northwest Pacific Ocean, and the error was within a reasonable range. Hence, this method can realize accurate observations of mesoscale eddies in the Northwest Pacific region. ECN provides high-resolution data of the three-dimensional temperature structure of mesoscale eddies, which is very important for improving the prediction accuracy of the three-dimensional temperature structure of mesoscale eddies.

However, SST, sea level wind field and other information will affect the accuracy of the derived three-dimensional temperature structure of mesoscale eddies. Therefore, further improving the accuracy of the proposed method for the temperature structure inversion of mesoscale eddies is the focus of future work.

References

Ali M M, Jagadeesh P S V, Lin I I, et al. 2012. A neural network approach to estimate tropical cyclone heat potential in the Indian Ocean. IEEE Geoscience and Remote Sensing Letters, 9(6): 1114–1117, doi: 10.1109/LGRS.2012.2190491

Ali M M, Swain D, Weller R A. 2004. Estimation of ocean subsurface thermal structure from surface parameters: a neural network approach. Geophysical Research Letters, 31(20): L20308, doi: 10.1029/2004GL021192

Alvera-Azcárate A, Barth A, Rixen M, et al. 2005. Reconstruction of incomplete oceanographic data sets using empirical orthogonal functions: application to the Adriatic Sea surface temperature. Ocean Modelling, 9(4): 325–346, doi: 10.1016/j.ocemod.2004.08.001

Barcelo-Llull B, Pascual A, Mason E, et al. 2018. Comparing a multivariate global ocean state estimate with high-resolution *in situ* data: an anticyclonic intrathermocline eddy near the canary islands. Frontiers in Marine Science, 5: 66, doi: 10.3389/fmars.2018.00066

Barth A, Alvera-Azcárate A, Licer M, et al. 2020. DINCAE 1.0: a convolutional neural network with error estimates to reconstruct sea surface temperature satellite observations. Geoscientific Model Development, 13(3): 1609–1622, doi: 10.5194/gmd-13-1609-2020

Corchado J M, Aiken J. 2002. Hybrid artificial intelligence methods in oceanographic forecast models. IEEE Transactions on Systems, 32(4): 307–313

de Boyer Montégut C, Madec G, Fischer A S, et al. 2004. Mixed layer depth over the global ocean: an examination of profile data and a profile-based climatology. Journal of Geophysical Research: Oceans, 109(C12): C12003, doi: 10.1029/2004JC002378

Ducournau A, Fablet R. 2016. Deep learning for ocean remote sensing: an application of convolutional neural networks for super-resolution on satellite-derived SST data. In: Proceedings of the 9th IAPR Workshop on Pattern Recogniton in Remote Sensing. Cancun, Mexico: IEEE

Fox D N, Teague W J, Barron C N, et al. 2002. The Modular Ocean Data Assimilation System (MODAS). Journal of Atmospheric and Oceanic Technology, 19(2): 240–252, doi: 10.1175/1520-0426(2002)019<0240:TMODAS>2.0.CO;2

Ge Xuyang, Wang Wanqiu, Kumar A, et al. 2017. Importance of the vertical resolution in simulating SST diurnal and intraseasonal

variability in an oceanic general circulation model. Journal of Climate, 30(11): 3963–3978, doi: 10.1175/JCLI-D-16-0689.1

Goni G, Kamholz S, Garzoli S, et al. 1996. Dynamics of the Brazil-Malvinas Confluence based on inverted echo sounders and altimetry. Journal of Geophysical Research: Oceans, 101(C7): 16273–16289, doi: 10.1029/96JC01146

Guinehut S, Dhomps A L, Larnicol G, et al. 2012. High resolution 3-D temperature and salinity fields derived from *in situ* and satellite observations. Ocean Science, 8(5): 845–857, doi: 10.5194/os-8-845-2012

Han Mingxu, Feng Yuan, Zhao Xueli, et al. 2019. A convolutional neural network using surface data to predict subsurface temperatures in the Pacific Ocean. IEEE Access, 7: 172816–172829, doi: 10.1109/ACCESS.2019.2955957

Hinton G E, Salakhutdinov R R. 2006. Reducing the dimensionality of data with neural networks. Science, 313(5786): 504–507, doi: 10.1126/science.1127647

LeCun Y, Bengio Y, Hinton G. 2015. Deep learning. Nature, 521(7553): 436–444, doi: 10.1038/nature14539

Lima E, Sun Xin, Dong Junyu, et al. 2017. Learning and transferring convolutional neural network knowledge to ocean front recognition. IEEE Geoscience and Remote Sensing Letters, 14(3): 354–358, doi: 10.1109/LGRS.2016.2643000

Liu Qinyan, Zhou Wen. 2010. Relationship between typhoon activity in the northwestern Pacific and the up-per-ocean heat content on interdecadal time scale. Journal of Tropical Oceanography, 29(6): 8–14

Long J, Shelhamer E, Darrell T. 2015. Fully convolutional networks for semantic segmentation. In: Proceedings of 2015 IEEE Conference on Computer Vision and Pattern Recognition. Boston, MA, USA: IEEE, 640–651

Lu Wenfang, Su Hua, Yang Xin, et al. 2019. Subsurface temperature estimation from remote sensing data using a clustering-neural network method. Remote Sensing of Environment, 229: 213–222, doi: 10.1016/j.rse.2019.04.009

Mandal S, Rao S, Raju D H. 2005. Ocean wave parameters estimation using backpropagation neural networks. Marine Structures, 18(3): 301–318, doi: 10.1016/j.marstruc.2005.09.002

Pun I F, Lin I I, Ko D S. 2014. New generation of satellite-derived ocean thermal structure for the western North Pacific typhoon intensity forecasting. Progress in Oceanography, 121: 109–124, doi: 10.1016/j.pocean.2013.10.004

Pun I F, Lin I I, Wu C R, et al. 2007. Validation and application of altimetry-derived upper ocean thermal structure in the western North Pacific Ocean for typhoon-intensity forecast. IEEE Transactions on Geoscience and Remote Sensing, 45(6): 1616–1630, doi: 10.1109/TGRS.2007.895950

Pun I F, Price J F, Jayne S R. 2016. Satellite-derived ocean thermal structure for the North Atlantic Hurricane Season. Monthly Weather Review, 144(3): 877–896, doi: 10.1175/MWR-D-15-0275.1

Rao A D, Joshi M, Jain I, et al. 2010. Response of subsurface waters in the eastern Arabian Sea to tropical cyclones. Estuarine, 89(4): 267–276

Shang Xiaodong, Xu Chi, Chen Guiying, et al. 2013. Review on mechanical energy of ocean mesoscale eddies and associated energy sources and sinks. Journal of Tropical Oceanography, 32(2): 24–36

Shay L K, Goni G J, Black P G. 2000. Effects of a warm oceanic feature on Hurricane Opal. Monthly Weather Review, 128(5): 1366–1383, doi: 10.1175/1520-0493(2000)128<1366:EOAWOF>2.0.CO;2

Shroyer E L, Rudnick D L, Farrar J T, et al. 2016. Modification of upper-ocean temperature structure by subsurface mixing in the presence of strong salinity stratification. Oceanography, 29(2): 62–71, doi: 10.5670/oceanog.2016.39

Song Tao, Jiang Jingyu, Li Wei, et al. 2020. A deep learning method with merged LSTM neural networks for SSHA prediction. IEEE Journal of Selected Topics in Applied Earth Observations and Remote Sensing, 13: 2853–2860, doi: 10.1109/JSTARS.2020.2998461

Su Hua, Li Wene, Yan Xiaohai. 2018. Retrieving temperature anomaly in the global subsurface and deeper ocean from satellite observations. Journal of Geophysical Research: Oceans, 123(1): 399–410, doi: 10.1002/2017JC013631

Su Hua, Yang Xin, Lu Wenfang, et al. 2019. Estimating subsurface thermohaline structure of the global ocean using surface remote sensing observations. Remote Sensing, 11(13): 1598, doi: 10.3390/rs11131598

Wu C C, Tu W T, Pun I F, et al. 2016. Tropical cyclone-ocean interaction in Typhoon Megi (2010)- A synergy study based on ITOP observations and atmosphere-ocean coupled model simulations. Journal of Geophysical Research: Atmospheres, 121(1): 153–167, doi: 10.1002/2015JD024198

Yang Yuting, Dong Junyu, Sun Xin, et al. 2016. Ocean front detection from instant remote sensing SST images. IEEE Geoscience and Remote Sensing Letters, 13(12): 1960–1964, doi: 10.1109/LGRS.2016.2618941

Yang Yuting, Dong Junyu, Sun Xin, et al. 2018. A CFCC-LSTM model for sea surface temperature prediction. IEEE Geoscience and Remote Sensing Letters, 15(2): 207–211, doi: 10.1109/LGRS.2017.2780843

Zhang Kun, Geng Xupu, Yan Xiaohai. 2020. Prediction of 3-D ocean temperature by multilayer convolutional LSTM. IEEE Geoscience and Remote Sensing Letters, 17(8): 1303–1307, doi: 10.1109/LGRS.2019.2947170

Zhao Ning, Han Zhen. 2015. A simulation model of seawater vertical temperature by using back-propagation neural network. Polish Maritime Research, 22(S1): 82–88, doi: 10.1515/pomr-2015-0037